ELSEVIER

Journal of Quantitative Spectroscopy & Radiative Transfer 92 (2005) 129–141

Journal of Quantitative Spectroscopy & Radiative Transfer

www.elsevier.com/locate/jqsrt

The simulation of infrared bands from the analyses of rotational spectra: the $2\nu_9-\nu_9$ and $\nu_5-\nu_9$ hot bands of HNO_3

D.T. Petkie[a], P. Helminger[b], B.P. Winnewisser[c], M. Winnewisser[c], R.A.H. Butler[d], K.W. Jucks[e], F.C. De Lucia[c,*]

[a] *Department of Physics, Wright State University, Dayton, OH 45435, USA*
[b] *Department of Physics, University of South Alabama, Mobile, AL 36688, USA*
[c] *Department of Physics, The Ohio State University, Columbus, OH 43210, USA*
[d] *Jet Propulsion Laboratory, California Institute of Technology, Pasadena, CA 91109-8099, USA*
[e] *Smithsonian Astrophysical Observatory, Cambridge, MA 02138, USA*

Received 4 August 2003; accepted 13 March 2004

Abstract

The results of millimeter and submillimeter wave rotational spectroscopy are used to simulate the complex structure of the $2\nu_9-\nu_9$ (438 cm^{-1}) and $\nu_5-\nu_9$ (421 cm^{-1}) hot bands. The comparison data were obtained with a high-resolution Bruker FTIR. The combination of the quality of these data and the complexity of the spectra of these interacting states represents a stringent test for the simulation. It is shown that the agreement is very good and that this approach is generally advantageous. From this simulation, the ratios of the transition dipole moments for the $2\nu_9-\nu_9$ and $\nu_5-\nu_9$ hot bands with respect to the ν_9 fundamental band were found to be 1.38(11) and 0.67(20), respectively. Using these results, the calculated integrated band intensities for the hot bands at 296 K were determined to be $S_v(2\nu_9-\nu_9)=1.63\times10^{-18}$ $cm^{-1}/(mol\ cm^{-2})$ and $S_v(\nu_5-\nu_9)=0.36\times10^{-18}$ $cm^{-1}/(mol\ cm^{-2})$. These results were used to successfully simulate high-resolution stratospheric spectra obtained from a balloon flight of the FIRS-2 spectrometer. The more general problem of the rotation–vibration database and the optimal use of both microwave and infrared data to define it is discussed. It is concluded that it is best if the combination of data takes place at the level of the original spectra.

Keywords: HNO_3; Hot band intensities; Infrared spectra

* Corresponding author. Tel: +1-614-688-4774; fax: +1-614-292-7557.
E-mail address: fcd@mps.ohio-state.edu (F.C. De Lucia).

0022-4073/$ - see front matter © 2004 Elsevier Ltd. All rights reserved.
doi:10.1016/j.jqsrt.2004.03.003

1. Introduction

With the increase in resolution of infrared methods and the broadening of the spectral region available for measurements with microwave techniques, the information content from the two spectral regions has come to overlap. This overlap is often complementary, but in many cases it has not been fully exploited because of the size and complexity of the databases and, more importantly, of the fundamental spectral data upon which they are based.

Recently, we have used microwave measurements as the basis for a calculation of the rotational structure of the $\upsilon_9 = 2/\upsilon_5 = 1$ interacting dyad which lies about 900 cm^{-1} above the ground state [1]. Earlier, we reported the analysis of $\upsilon_9 = 1$ [2,3] and more recently we have reported updated analyses for the ground and $\upsilon_9 = 1$ vibrational states [4]. In this paper we use these results, along with an intensity calculation, to simulate a high-resolution FTIR laboratory spectrum of the $2\nu_9 - \nu_9$ and $\nu_5 - \nu_9$ hot bands near 22 μm (438 and 421 cm^{-1}, respectively). This provides a particularly stringent test of the usefulness of the simulation because (1) of the high resolution of the infrared data being simulated, (2) the intensities can also be tested because the infrared spectrum was taken at a single well-defined temperature in the laboratory, and (3) of the complex interactions between $\upsilon_9 = 2$ and $\upsilon_5 = 1$. From the present simulation we were able to determine the relative intensities of the hot bands compared to the fundamental band, which will improve modeling of atmospheric emission observations [5].

2. Comparisons and combination of infrared and microwave results

We have recently published a calculation of the rotational energy level structure of the $\upsilon_9 = 2/\upsilon_5 = 1$ interacting dyad which, along with the ground state rotational structure, gives rise to the strong and complex structure near 11 μm (890 cm^{-1}) [1]. In addition to the considerable interest of both laboratory spectroscopists and atmospheric scientists, we were interested in this case because it presented a particularly rigorous challenge to the synthesis of 'infrared' energy levels from 'microwave' data. This is because highly accurate infrared data and analyses for these states existed to high J and also because of the complex mixing of the $\upsilon_9 = 2$ and $\upsilon_5 = 1$ states [6–8].

The comparison and optimal combination of infrared and microwave data are not straightforward. Most commonly, both communities publish spectral constants that result from fits to their respective data, or in some cases analyses with some data from the other regime included. These constants represent the last in a chain of data reductions and the most compact representation of the results. However, because of model differences (e.g. the constants selected for inclusion in the Hamiltonian) and correlations among the constants, it is not always enlightening to compare only these spectral constants. Likewise, it is not always possible to use these constants to reproduce either energy levels or spectral details because correlations of the fit are commonly not published and prevent reliable uncertainties from being established.

It is more common and useful to compare calculated energy levels. The comparison of the $\upsilon_9 = 2$ and $\upsilon_5 = 1$ infrared and microwave analyses were done by comparing the 'observed' (i.e. those obtained from the spectral data via a fitting of combination differences, etc.) infrared levels with those calculated from an analysis of a microwave data set. This agreement was found to be very good [1]. More specifically, the distribution of differences between (1) the *predictions* from the microwave

analysis and the 'observed' infrared energy levels, and (2) the fit of the 'observed' energy levels to a model were very similar.

Our ability to obtain this good agreement was, however, in some sense fortuitous and further illustrates the need to use spectral data directly. The very good agreement between the 'infrared' and 'microwave' energy levels, in fact, requires the inclusion of the microwave rotational ground state constants (or data) in the 'infrared' analyses. Because of the selection rule, $\Delta J = 0, \pm 1$, the energy of a level at high J must be calculated from either microwave or infrared data by the addition (and subtraction) of many measured frequencies or wavenumbers, thus propagating systematic and random experimental errors and making the error in the energy of a high J state much greater than that of a typical observation. However, because the microwave frequencies are typically 100 times more accurate, the calculation of an energy level from the accumulated error in the microwave ground state energy level structure (which is still small) and a *single* infrared ro-vibration wavenumber yield essentially the error in the rovibration wavenumber itself, not the total of the accumulated error from addition of many infrared line positions.

3. Methods of the simulation

For the simulations reported here we use the results of the microwave analyses of the pure rotational spectra of the $\upsilon_9 = 2$, $\upsilon_5 = 1$, $\upsilon_9 = 1$ and ground states we have recently reported [1,4]. The pure rotational spectra of the vibrationally excited states exhibit a torsional splitting, requiring an internal axis system (IAS) Hamiltonian with torsional parameters to accurately reproduce the spectra. Since the ground state lines do not exhibit an observable torsional splitting, the principal axis system (PAS) Hamiltonian was used in fitting this spectrum. When synthesizing the infrared spectrum, a consistent choice for the axis system must be made with both vibrational states either being in the PAS or IAS to properly calculate the matrix elements of the transition dipole moment. Since the ~ 2 MHz ($0.00007\ \mathrm{cm}^{-1}$) torsional splitting is not resolvable in the υ_9 fundamental infrared band, we chose to use the ground state and $\upsilon_9 = 1$ PAS analyses of Ref. [4]. While the $\upsilon_9 = 1$ PAS analysis does not contain transitions effected by the torsional splitting (mainly b-type transitions), it does contain an extensive set of a-type transitions that are sufficient to model the fundamental infrared band. While torsional splitting is not resolvable in the fundamental ν_5 or $2\nu_9$ bands (torsional splitting of ~ 35 MHz ($0.0012\ \mathrm{cm}^{-1}$) and ~ 50 MHz ($0.0017\ \mathrm{cm}^{-1}$), respectively) or in the $2\nu_9-\nu_9$ and $\nu_5-\nu_9$ hot bands, Coudert and Perrin [8] did notice a small difference in the statistical distribution of deviations in fitting the $\upsilon_5 = 1$ and $\upsilon_9 = 2$ experimentally determined infrared energy levels that was attributed to the large amplitude torsional motion. On the other hand, much of the pure rotational data from the $\upsilon_5 = 1/\upsilon_9 = 2$ dyad cannot be accurately modeled without an IAS-like Hamiltonian, particularly transitions with asymmetry splitting. Therefore, for the simulation of the $2\nu_9-\nu_9$ and $\nu_5-\nu_9$ hot bands, the $\upsilon_5 = 1/\upsilon_9 = 2$ dyad "artificial splitting" IAS analysis (Fermi resonance constant $F_o = 0$, with two sets of torsional parameters) of Ref. [1] and the $\upsilon_9 = 1$ IAS analysis of Ref. [4] were used. Pickett's SPCAT program [9] was used to predict the frequencies and intensities of the transitions in each band.

The FTIR spectrum used for comparison was recorded at Giessen and first reported in Ref. [7]. The experimental parameters are given in Table 1. The spectrum was calibrated using H_2O and CO_2 lines from the HITRAN database and was zero-filled by a factor of eight (leading to the sampling

Table 1
FTIR experimental parameters

Parameter	Value	FWHM in simulation (cm^{-1})
Maximum optical path difference	485 cm	0.00124
Aperture diameter	2 mm	
Collimator focal length	400 mm	0.00132
Pressure	9 Pa	0.00014
Temperature	297 K	0.00067

interval of 9.41×10^{-5} cm^{-1}) so that each line would have a sufficient number of points to allow accurate modeling of the spectrum.

The transmission spectrum was calculated using the following expression:

$$\tau(\tilde{\nu}) = ILS(\tilde{\nu}) \otimes \prod_i \exp\left((-nL)^i \mu_c^2 \sum_{ab} I_{i,ab} f_{i,ab}(\tilde{\nu} - \tilde{\nu}_{i,ab} - \tilde{\nu}_i) \right), \quad (1)$$

where $\tilde{\nu}$ is the wavenumber, $ILS(\tilde{\nu})$ is the instrumental function; $\otimes$ indicates a convolution; n is the number density in the absorption path L; ${}^i\mu_c$ is the c-type transition dipole moment for band i; $I_{i,ab}$ is the line intensity and $\tilde{\nu}_{i,ab}$ is the line position relative to the band origin for a specific transition ab in band i calculated by SPCAT; $f_{i,ab}(\tilde{\nu} - \tilde{\nu}_{i,ab} - \tilde{\nu}_i)$ is the Voigt profile; and $\tilde{\nu}_i$ is the band origin for each band. In this study the product of the concentration and path length is a common factor when comparing the relative intensities of the bands and therefore not important. The dominant contribution to line broadening was the instrumental line shape that was modeled after the functions of Refs. [10,11], which is a convolution of a sinc function (finite path difference) and a boxcar (finite source aperture) function. These functions were calculated based on the experimental parameters of Table 1 and were not fit for in the analysis. Since both the aperture contribution and Doppler widths are a function of the wavenumber, the center band of the synthesis, ~ 430 cm^{-1}, was used in calculating the widths of each. The pressure broadening parameters were calculated based on the temperature and pressure in Table 1 along with a self-broadening coefficient of 0.80 cm^{-1}/atm from Refs. [12,13]. Table 1 also shows the line widths calculated for each broadening mechanism in terms of the full-width at half-maximum (FWHM) in simulation.

A total of six parameters were fit that correspond to the overall intensity factors, proportional to ${}^i\mu_c^2$, and the band centers, $\tilde{\nu}_i$, for each band of the three bands. The portions of the spectrum that were selected as being most sensitive to the quality of the simulation, and thus fit quantitatively, were the dominant Q-branches of the hot bands (~ 421 and ~ 438 cm^{-1}) including the portion of the P-branch from the fundamental band in the region of the $2\nu_9-\nu_9$ Q-branch. The fundamental band and the $2\nu_9-\nu_9$ hot band were fit simultaneously followed by a fit of the $\nu_5-\nu_9$ hot band with the other two bands held fixed. The regions fit centered on the hot-band Q branches are shown in Figs. 1 and 2. Individual water lines were satisfactorily removed by independently fitting each line to a Gaussian line shape. Because of the large number of points created by zero-filling and computer program limitations, the size of the largest spectral window we could fit was ~ 5 cm^{-1}. While we could fit larger spectral windows by decreasing the zero-filling factor, the quality of the fit deteriorated slightly.

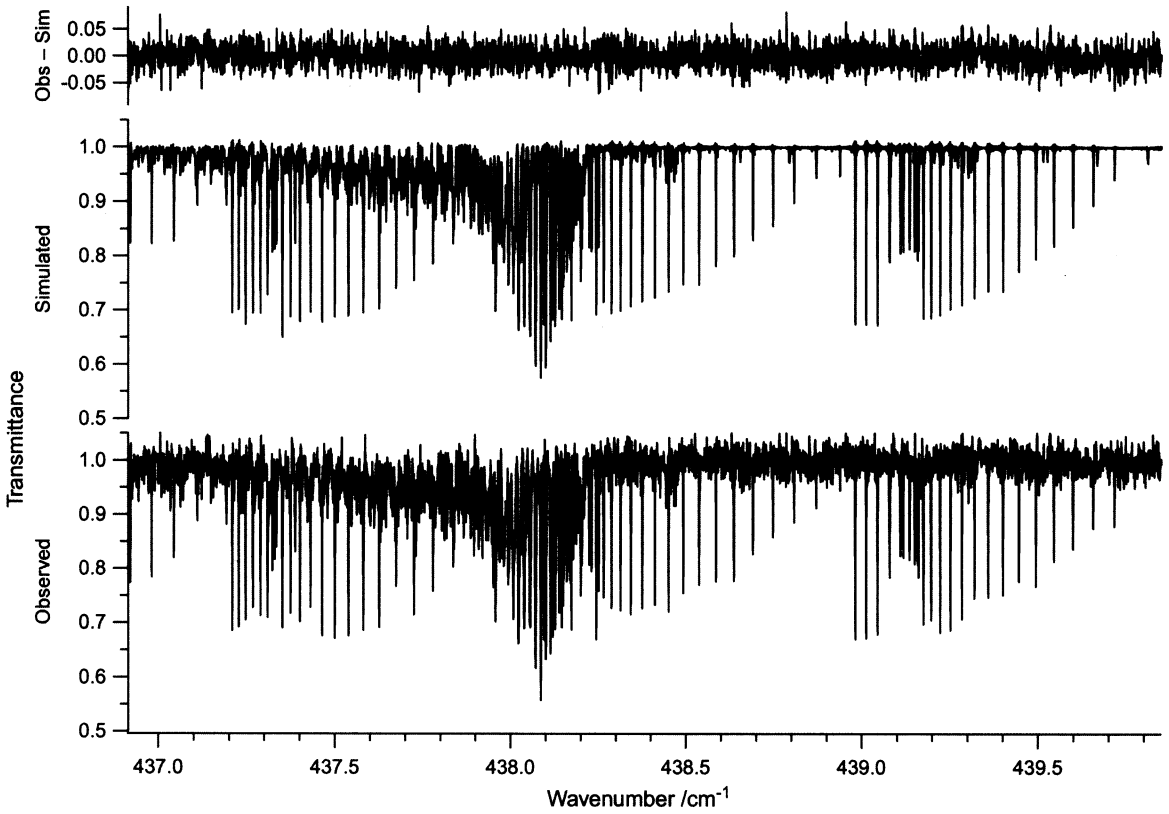

Fig. 1. The region around the Q-branch of the $2\nu_9-\nu_9$ hot band near 438 cm^{-1}. In addition to the dense cluster of lines which make up the Q-branch, significant spectral intensity in this region comes from the P-branch of the ν_9 fundamental, whose origin is near 458 cm^{-1}. Three of these P-branch clusters, separated by $\sim$ 1 cm^{-1}, can be seen in the figure. This region was used in a least squares fit of the synthetic spectrum to the laboratory spectrum to determine the relative intensity of the two bands. The laboratory spectrum, fitted synthetic spectrum and the residuals are shown with identical vertical scales.

4. Results and discussion

As described above, two spectral regions of $\sim$ 5 cm^{-1} were fit with the full resolution achievable. This determined the overall intensity factors for the two hot bands with respect to the fundamental band. The results of these fits are shown in Figs. 1 and 2 and the relative intensity factors are given in Table 2. These figures show the Q-branch of each hot band along with segments of the P-branch from the fundamental band. Figs. 3 and 4 display the simulation over a narrower spectral region around each hot band Q-branch and show excellent agreement between the observed and simulated spectrum.

4.1. Determination of intensity factors

The uncertainty in the ratio of the intensity factors of $\sim$ 6% was arrived at by considering the statistical uncertainty of the least squares fit ($\sim$ 0.5%) and by varying several parameters in the

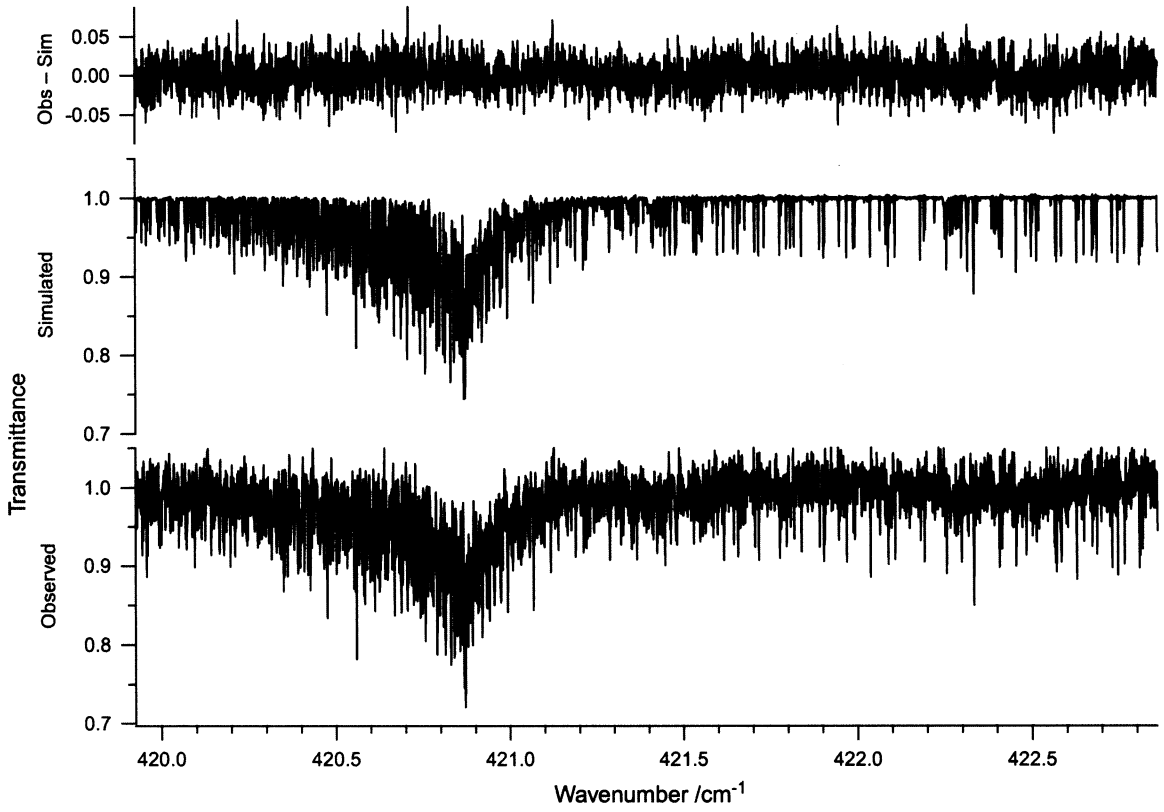

Fig. 2. The region around the Q-branch of the v_5–v_9 hot band near 421 cm^{-1}. In addition to the dense cluster of lines which make up the Q-branch, some spectral intensity in this region comes from the P-branch of the v_9 fundamental, whose origin is near 458 cm^{-1}. Since these P-branch clusters are at higher J, they are weaker and less distinct than those shown in Fig. 1. Because of this, the intensity of the v_9 fundamental was determined in the least squares fit of the region shown in Fig. 1 and was held fixed when fitting for the relative intensity of the v_5–v_9 hot band shown in this figure. The laboratory spectrum, fitted synthetic spectrum and the residuals are shown with identical vertical scales.

analysis, which included the aperture diameter, the temperature, and the location of the $\sim 5\ cm^{-1}$ spectral window. The line shape has the largest contribution to the uncertainties ($\sim 3.5\%$), followed by the temperature ($\sim 1.5\%$), with the choice of spectral window having the smallest ($\sim 0.5\%$). The relative intensity of the hot bands to each other has a lower uncertainty than when comparing either hot band to the fundamental. This is not surprising for two reasons. The first is that each hot band has the same lower state, making the uncertainty in the temperature less significant. Secondly, the intensity of each hot band is mainly determined by the fitting of the partially resolved Q-branch structure compared to resolved P-branches transitions of the fundamental band. This leads to the uncertainty that is attributable to variations in the line shape, with the uncertainty being reduced when comparing the hot bands to one another since the shape of the partially resolved hot band Q branches are similar and correlated in the analysis.

In the study of the fundamental band by Sirota et al. [14], the first order c-type transition dipole moment was determined to be $\pm(0.2561\pm0.0021)$ Debye by fitting the intensity of 38 P and R branch

Table 2
Intensity ratio factors

Band intensity factors	Experimental	Projected[a]
$\left\lvert \frac{^{2\nu 9-\nu 9}\mu_c}{^{\nu 9}\mu_c} \right\rvert^2$	1.31 ± 0.08	1.18
$\left\lvert \frac{^{\nu 5-\nu 9}\mu_c}{^{\nu 9}\mu_c} \right\rvert^2$	1.05 ± 0.06	0.82
$\left\lvert \frac{^{2\nu 9-\nu 9}\mu_c}{^{\nu 5-\nu 9}\mu_c} \right\rvert^2$	1.25 ± 0.02	1.43
$\left\lvert \frac{^{2\nu 9-\nu 9}\mu_c}{^{\nu 9}\mu_c} \right\rvert^2 + \left\lvert \frac{^{\nu 5-\nu 9}\mu_c}{^{\nu 9}\mu_c} \right\rvert^2$	2.36 ± 0.14	2.00

[a]Projected harmonic oscillator values assuming $|^{2\nu 9-\nu 9}\mu_c^0/^{\nu 9}\mu_c|^2 = 2$ and $|^{\nu 5-\nu 9}\mu_c^0/^{\nu 9}\mu_c|^2 = 0$ and a 58.9% mixing of the vibrational wave functions of the $\upsilon_5 = 1$ and $\upsilon_9 = 2$ due to a strong Fermi resonance [1].

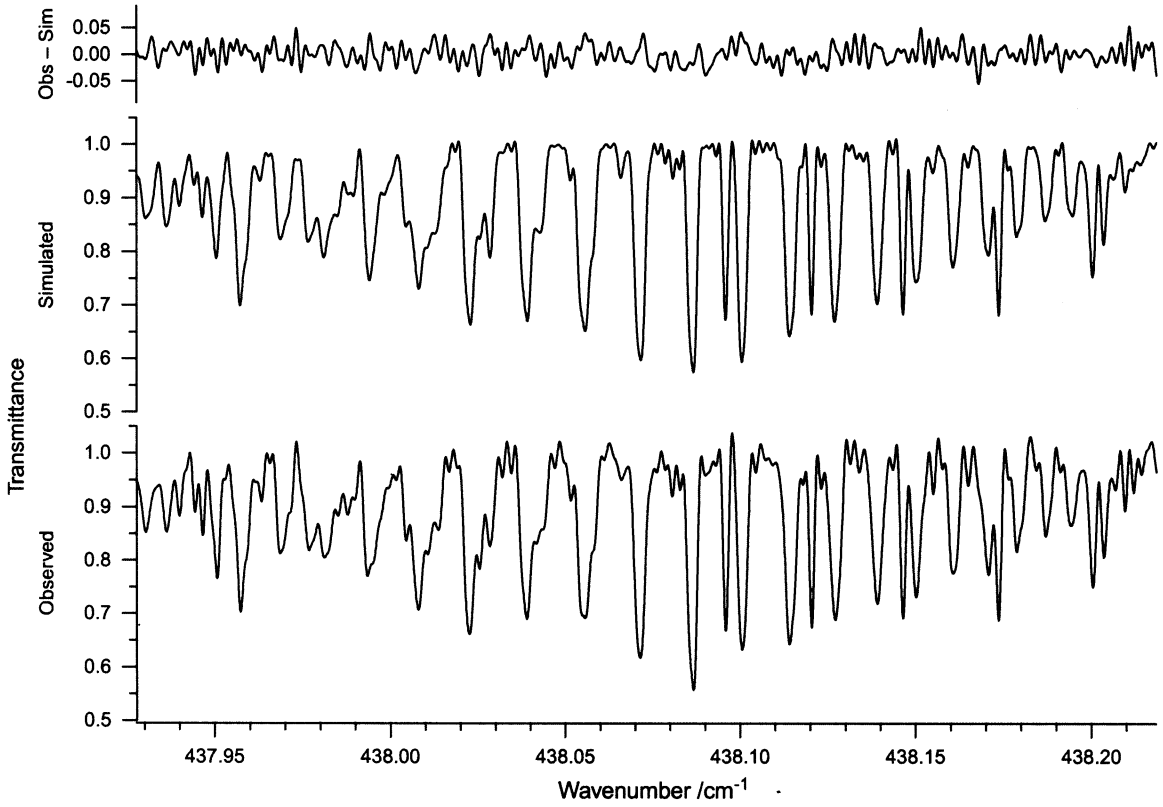

Fig. 3. An expansion of the central region of the Q-branch of the $2\nu_9-\nu_9$ hot band near 438 cm^{-1}. The line positions and shapes are accurately predicted. All vertical scales are identical and the rms variation of the residual is $\sim 2\%$.

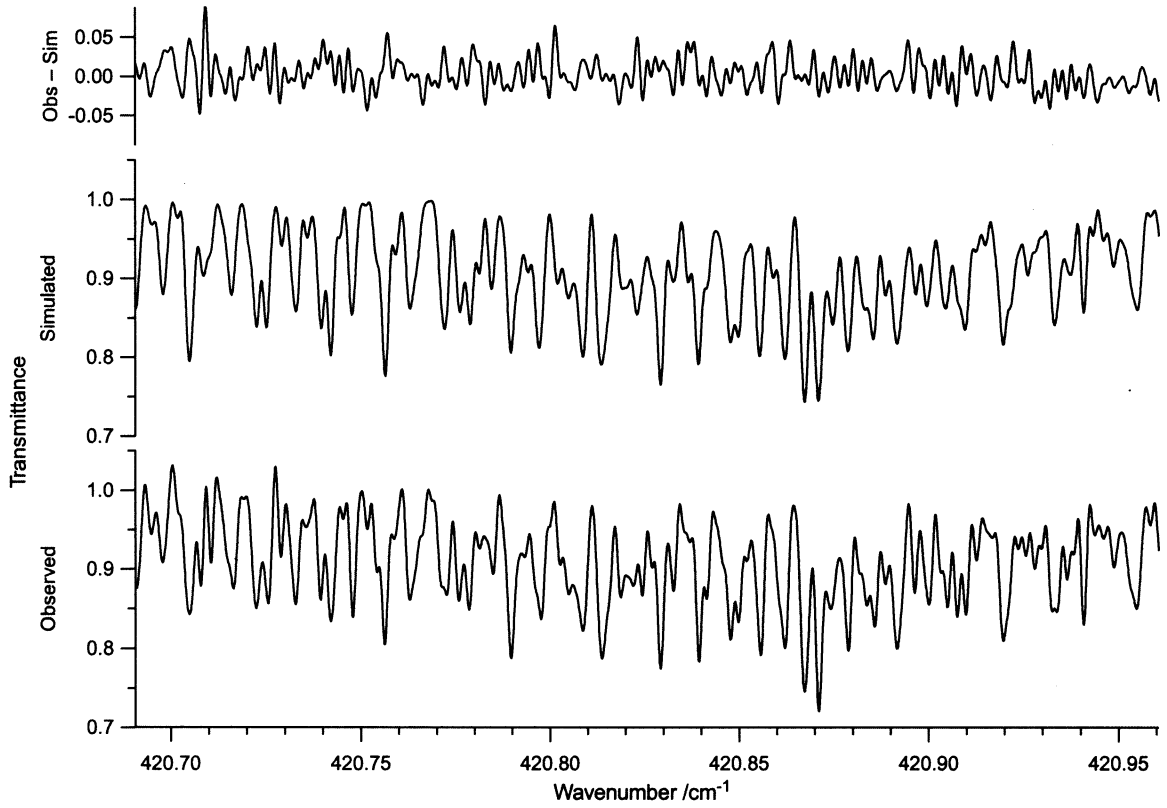

Fig. 4. An expansion of the central region of the Q-branch of the v_5–v_9 hot band near 421 cm^{-1}. The line positions and shapes are accurately predicted. All vertical scales are identical and the rms variation of the residual is $\sim 2\%$.

transitions, with no need for higher order terms. While the largest spectral window we could fit was limited to $\sim 5\ cm^{-1}$, we synthesized the entire ~ 416–$492\ cm^{-1}$ spectral window that is shown in Fig. 5. The residuals show no need for higher order terms in the transition dipole moment operator. Additionally, the residuals show two Q branches of other hot bands, $v_8 + v_9 - v_8$ at $\sim 442.5\ cm^{-1}$ and an unidentified band at $\sim 453\ cm^{-1}$ [7]. The large residuals in the fundamental Q-branch region near $\sim 458\ cm^{-1}$ are due to the difficulty in simulating the near opaque nature of this region, the sum of all other hot bands, and also possibly line mixing.

4.2. Transition dipole moments

The intensity ratio factors of Table 2 were used to calculate the perturbed and unperturbed transition moments that are shown in Table 3. Since the band intensity is proportional to the square of the transition moment, the perturbed moments were determined by simply taking the square root of the observed intensity ratios and multiplying by the transition moment of the fundamental band of Ref. [14]. To determine the unperturbed transition dipole moments, we assumed non-zero transition moments for each band and fixed the mixing coefficient of the vibrational states to 58.9% [1], which

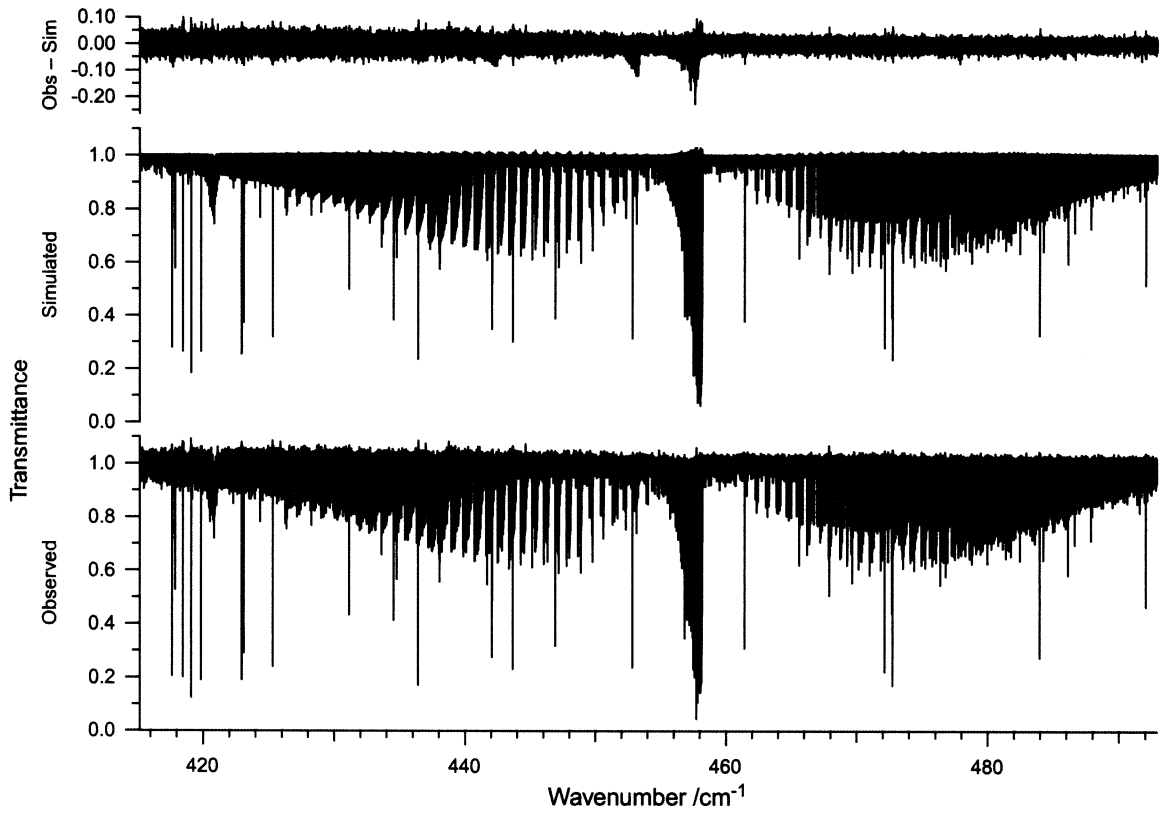

Fig. 5. The entire ν_9 band is shown along with several hot bands. While the relative intensities were determined in ~ 5 cm^{-1} spectral windows near the 438 and 421 cm^{-1} hot band locations, the entire spectral window from ~ 416 to 492 cm^{-1} was accurately synthesized and shows no need for J/K dependent expansion of the c-type transition dipole moment. The residual indicates the location of two additional hot bands, $\nu_8+\nu_9-\nu_9$ at ~ 442.5 cm^{-1} and an unidentified band at ~ 453 cm^{-1} [7]. The large residuals near 458 cm^{-1} are due to the difficulty in simulating a near opaque region containing further weak hot bands along with the possibility of line mixing. The rms residual for the entire region is $\sim 2\%$ and is slightly larger at the lower end of the spectrum due to a lower S/N associated with the laboratory spectrum.

leads to the following equations [15]:

$$a^2\left|\frac{^{2\nu9-\nu9}\mu_c^0}{^{\nu9}\mu_c}\right|^2+b^2\left|\frac{^{\nu5-\nu9}\mu_c^0}{^{\nu9}\mu_c}\right|^2\pm 2ab\sqrt{\left|\frac{^{2\nu9-\nu9}\mu_c^0}{^{\nu9}\mu_c}\right|^2\left|\frac{^{\nu5-\nu9}\mu_c^0}{^{\nu9}\mu_c}\right|^2}=\left|\frac{^{2\nu9-\nu9}\mu_c}{^{\nu9}\mu_c}\right|^2, \tag{2}$$

$$b^2\left|\frac{^{2\nu9-\nu9}\mu_c^0}{^{\nu9}\mu_c}\right|^2+a^2\left|\frac{^{\nu5-\nu9}\mu_c^0}{^{\nu9}\mu_c}\right|^2\mp 2ab\sqrt{\left|\frac{^{2\nu9-\nu9}\mu_c^0}{^{\nu9}\mu_c}\right|^2\left|\frac{^{\nu5-\nu9}\mu_c^0}{^{\nu9}\mu_c}\right|^2}=\left|\frac{^{\nu5-\nu9}\mu_c}{^{\nu9}\mu_c}\right|^2, \tag{3}$$

where a^2 is the mixing coefficient of 0.589 ($a^2+b^2=1$) and the unperturbed and fitted transition dipole moment ratios are on the left- and right-hand side of the expressions, respectively. The results for the unperturbed transition moments are also shown in Table 3. The unperturbed transition moment for the $2\nu_9-\nu_9$ hot band is higher than the projected harmonic oscillator value of $\approx\sqrt{2}|^{\nu9}\mu_c|$ [16,17], while the transition moment of the $\nu_5-\nu_9$ hot band was not determinable, as expected for a difference band.

Table 3
Transition moments (Debye)

Transition moment	Experimental	Projected[a]
$\lvert^{v9}\mu_c\rvert$, Ref. [14]	0.2561 ± 0.0021	—
Perturbed[b]		
$\lvert^{2v9-v9}\mu_c\rvert$	0.293 ± 0.009	0.278
$\lvert^{v5-v9}\mu_c\rvert$	0.262 ± 0.008	0.232
Unperturbed[c]		
$\lvert^{2v9-v9}\mu_c^0\rvert$	0.393 ± 0.033	0.362
$\lvert^{v5-v9}\mu_c^0\rvert$	0.014 ± 0.032	0.000

[a]Projected harmonic oscillator values assuming $|^{2v9-v9}\mu_c^0/^{v9}\mu_c|^2 = 2$ and $|^{v5-v9}\mu_c^0/^{v9}\mu_c|^2 = 0$ and a 58.9% mixing of the vibrational wave functions of v_5 and $2v_9$ due to a strong Fermi Resonance [1].

[b]Assumes no Fermi mixing of the $J = 0$ levels (Fermi resonance constant $F_o = 0$).

[c]Assumes non-zero transition moments for each band with a fixed mixing coefficient of 58.9%. See text and Eqs. (2) and (3).

4.3. Integrated band intensities

The analyses of Refs. [1,4] and the perturbed transition dipole moments of Table 3 were used to generate a list of transition frequencies and intensities as well as the total band intensity for each band at 296 K. We used the same constraints as Sirota et al. [14], namely $J \leqslant 65$, $K_a \leqslant 60$, an intensity cutoff of 0.1×10^{-24} cm^{-1}/(mol cm^{-2}), maximum lower term value of 2000 cm^{-1}, and a maximum upper value of 2500 cm^{-1}. We used 0.989 for the isotopic abundance of $H^{14}N^{16}O_3$ and $Z_V(296\text{ K}) = 1.304$ and $Z_R(296\text{ K}) = 27343$ for the vibrational and rotational partition functions. The integrated band intensities at 296 K are $S_v(v_9) = 8.42 \times 10^{-18}$ cm^{-1}/(mol cm^{-2}), $S_v(2v_9-v_9) = 1.12 \times 10^{-18}$ cm^{-1}/(mol cm^{-2}), and $S_v(v_5-v_9) = 0.852 \times 10^{-18}$ cm^{-1}/(mol cm^{-2}).

5. Modeling of FIRS-2 atmospheric spectra

We have taken the calculated positions and strengths used to simulate these laboratory spectra to simulate high-resolution stratospheric spectra that span the entire 22 μm spectral region. These spectra were obtained from a balloon flight of the FIRS-2 spectrometer from the Harvard–Smithsonian Center for Astrophysics [18]. A sample of these spectra and the results of the simulation are shown in Fig. 6. These are thermal emission spectra taken at a resolution of 0.004 cm^{-1}. The data shown here are apodized with a von Hann function, resulting in a resolution of 0.008 cm^{-1}. The intensities and background of these spectra are obtained from blackbody and cold sky spectra. The spectrometer altitude was approximately 37 km and was observing through the limb of the atmosphere with a tangent altitude of approximately 20 km. All of the strong and broader lines in this spectrum are those of atmospheric water vapor. The $2v_9-v_9$ band is strongly overlapped by the P-branch lines of the fundamental band, as is also observed in the laboratory spectra. The calculated spectrum was produced using the line-by-line radiative transfer code developed to analyze the FIRS-2 balloon data [18].

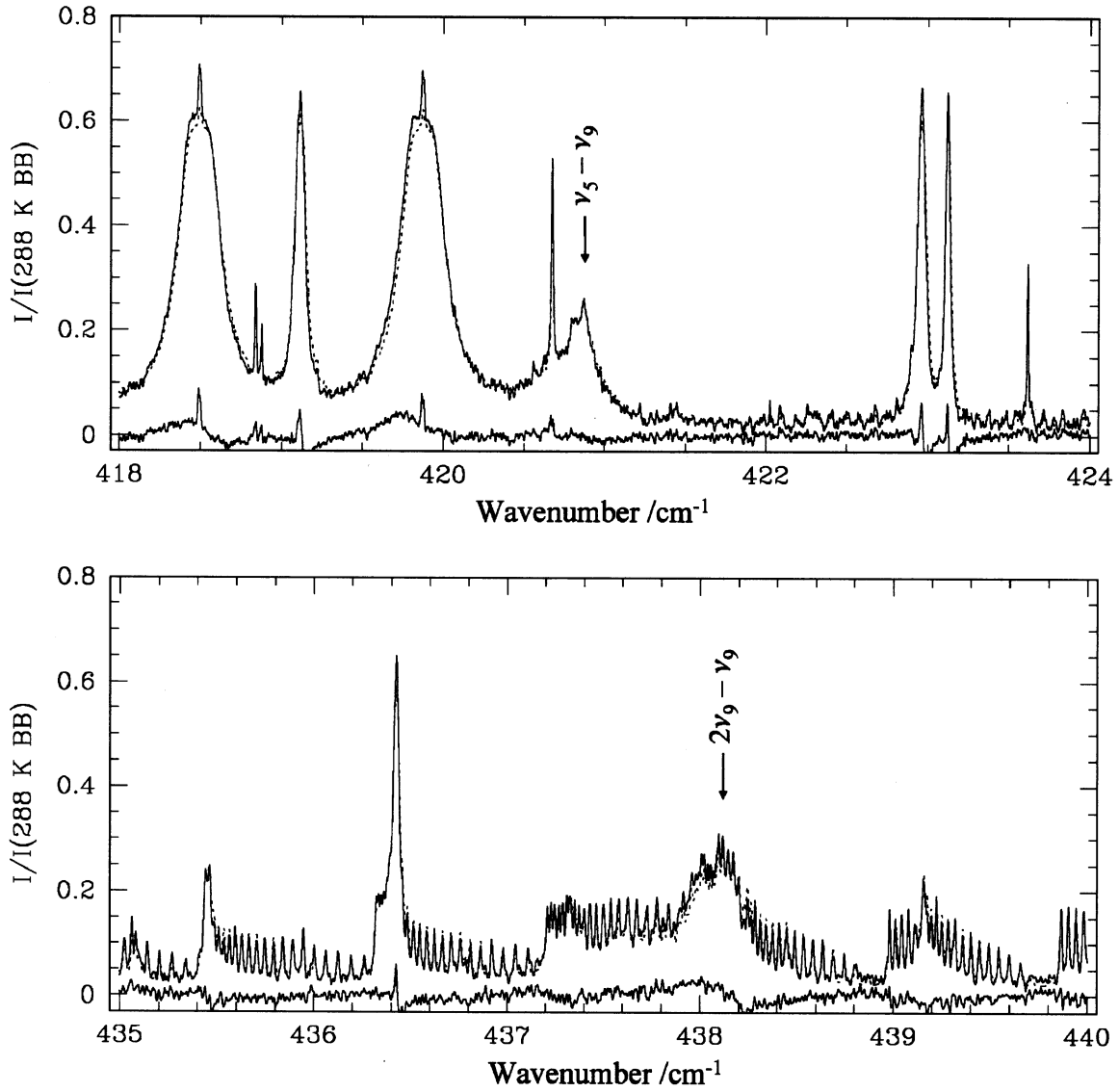

Fig. 6. The FIRS-2 balloon spectrum of the $\nu_5-\nu_9$ and $2\nu_9-\nu_9$ regions along with radiative transfer simulations of the bands. The upper solid trace of each panel is the observed balloon spectrum, the dashed trace is the simulated spectrum and the lower solid line is the residual (observed–simulated). This spectrum was obtained in limb viewing geometry with balloon altitude of 37 km and a tangent altitude of 20 km.

The residuals to the fit around the HNO_3 spectral features are all within the noise of the spectra. The largest residuals are near the cores of the water vapor lines. This results because the model is not correctly accounting for the water vapor in the vicinity of the balloon that is outgassing from the balloon and gondola. Even though these atmospheric data were obtained at much colder temperatures (roughly 226 K) than that used for the laboratory spectra, the relative strengths of the hot and fundamental bands are also consistent, which supports the relative strength determinations obtained from the analysis of the laboratory data.

6. Summary

We have shown in the case of the complex $2\nu_9-\nu_9$ and $\nu_5-\nu_9$ hot bands of HNO_3 near 22 μm that the rotational structure of the infrared spectrum as obtained by a high-resolution laboratory instrument can be simulated to high accuracy. By extension, this approach makes possible the simulation of spectra in many circumstances, including the analysis of spectrally based remote sensing instruments that was demonstrated here. While in this case the 'microwave' data was extensive enough to do this with great accuracy, more generally in cases where the infrared data and microwave data can both make significant contributions to the rotational analysis, it would be most advantageous to include both in a single combined weighted fit. However, to be able to do so requires access to the original measured line positions, not just to energy levels reduced from them. For HNO_3, the problem with the choice of axis systems in synthesizing the infrared spectrum illustrates why it is important to be able to start from empirical observations, in this case the spectra, rather than parameters derived from them that are model-dependent.

Acknowledgements

We would like to thank NASA for its support of this work.

References

[1] Petkie DT, Goyette TM, Helminger P, Pickett HM, De Lucia FC. The energy levels of the $\nu_5/2\nu_9$ dyad of HNO_3 from millimeter and submillimeter rotational spectroscopy. J Mol Spectrosc 2001;208:12–35.
[2] Crownover RL, Booker RA, De Lucia FC, Helminger P. The rotational spectrum of nitric acid the first 5 vibrational states. JQSRT 1988;40:39–46.
[3] Paulse CD, Coudert LH, Goyette TM, Crownover RL, Helminger P, De Lucia FC. Torsional splitting in the υ_9 band of nitric acid. J Mol Spectrosc 1996;177:9–18.
[4] Petkie DT, Helminger P, Butler RAH, Albert S, De Lucia FC. The millimeter and submillimeter spectra of the ground state and excited ν_9, ν_8, ν_7, and ν_6 vibrational states of HNO_3. J Mol Spectrosc 2003;218:127–30.
[5] Goldman A, Rinsland CP, Perrin A, Flaud JM. HNO_3 line parameters: 1996 HITRAN update and new results. JQSRT 1998;60:851–61.
[6] Perrin A, Jaouen V, Valentin A, Flaud JM, Camy-Peyret C. The ν_5 and $2\nu_9$ bands of nitric acid. J Mol Spectrosc 1993;157:112–21.
[7] Perrin A, Flaud JM, Camy-Peyret C, Winnewisser BP, Klee S, Goldman A, Murcray FJ, Blatherwick RD, Bonomo FS, Murcray DG, Rinsland CP. First analysis of the $3\nu_9-\nu_9$, $3\nu_9-\nu_5$, and $3\nu_9-2\nu_9$ bands of HNO_3: Torsional splitting in the ν_9 vibrational mode. J Mol Spectrosc 1994;166:224–43.
[8] Coudert LH, Perrin A. Accounting for the torsional splitting in the ν_5 and $2\nu_9$ bands of nitric-acid. J Mol Spectrosc 1995;172:352–68.
[9] Pickett HM. The fitting and prediction of vibration-rotation spectra with spin interactions. J Mol Spectrosc 1991;148:371–7.
[10] Davis SP, Abrams MC, Brault JW. Fourier transform spectrometry. San Diego: Academic Press; 2001.
[11] Zou QJ, Nemtchinov V, Varanasi P. An instrumental function and a non-linear least-squares multi-spectral-line-fitting algorithm applicable to FTS studies. JQSRT 2002;75:53–61.
[12] Brockman P, Bair CH, Allario F. High resolution spectral measurement of the nitric acid 11.3-μm band using tunable diode lasers. Appl Opt 1978;17:91–100.
[13] Zu L, Hamilton PA, Davies PB. Pressure broadening and frequency measurements of nitric acid lines in the 683 GHz region. JQSRT 2002;73:545–56.

[14] Sirota JM, Weber M, Reuter DC, Perrin A. HNO_3: absolute line intensities for the ν_9 fundamental. J Mol Spectrosc 1997;184:140–4.
[15] Wagner G, Winnewisser BP, Winnewisser M. The effects of a strong coriolis resonance on rovibrational line-intensities of $H^{13}CNO$. J Mol Spectrosc 1991;146:104–19.
[16] Maki A, Quapp W, Klee S. Intensities of hot-band transitions: HCN hot bands. J Mol Spectrosc 1995;171:420–34.
[17] Flaud J-M, Camy-Peyret C, Rinsland CP, Smith MA. Atlas of ozone spectral parameters from microwave to medium infrared. Boston: Academic Press; 1990.
[18] Johnson DG, Jucks KW, Traub WA, Chance KV. Smithsonian stratospheric far-infrared spectrometer and data reduction system. J Geophys Res-Atmos 1995;100:3091–106.